SUPPLEMENTAL FIGURES

Fig. S1 (related to Table 1). PtdIns*P* selectivity of selected SH2 domains and the Akt-PH domain. PtdIns*P* selectivity for each protein is as follows (from top to bottom): (A) Fyn-SH2: PIP_3 > $PI45P_2$ >> $PI34P_2$ ≈ $PI35P_2$ ≈ PI4P ≈ PI5P ≈ PI3P. (B) BMX-SH2: $PI45P_2$ > PIP_3 > $PI34P_2$ > $PI35P_2$ > PI5P ≈ PI4P ≈ PI3P. (C) ZAP70-cSH2: PIP_3 > $PI45P_2$ > $PI35P_2$ ≈ $PI35P_2$ > PI4P ≈ PI3P > PI5P. (D) PLCγ2-cSH2: PIP_3 > $PI45P_2$ >> $PI34P_2$ ≈ $PI35P_2$ ≈ PI4P ≈ PI5P ≈ PI3P (E) Btk-SH2: PIP_3 > $PI45P_2$ > $PI34P_2$ > $PI35P_2$ > PI4P ≈ PI3P > PI5P (F) Syk-cSH2: PIP_3 > $PI45P_2$ > $PI34P_2$ > $PI35P_2$ ≈ PI4P ≈ PI5P ≈ PI3P (G) Tensin1-SH2: PIP_3 >> $PI45P_2$ ≈ $PI34P_2$ > $PI35P_2$ > PI4P ≈ PI5P ≈ PI3P. (H) SPT6-cSH2: $PI45P_2$ ≈ PIP3 > PI5P > PI4P > PI3P > $PI35P_2$ > $PI34P_2$ (I) PTK6-SH2: $PI34P_2$ ≈ PIP3 ≈ $PI35P_2$ > $PI45P_2$ ≈ PI5P > PI4P > PI3P. (J) YES1-SH2: $PI45P_2$ > PIP3 > $PI34P_2$ > $PI35P_2$ > PI5P ≈ PI4P ≈ PI3P. (K) RASA1-nSH2: PIP3 ≈ $PI45P_2$ > $PI35P_2$ > $PI34P_2$ > PI5P > PI4P ≈ PI3P. (L) PDK1-PH: $PI34P_2$ ≈ PIP_3 >> $PI45P_2$ > $PI35P_2$ > PI5P ≈ PI4P ≈ PI3P.

PtdIns*P* selectivity of the Akt-PH domain is shown for comparison.

SPR measurements were performed in 20 mM Tris-HCl, pH 7.4, containing 0.16 M KCl. POPC/POPS (80:20) and POPC/POPS/PtdIns*P* (77:20:3) vesicles were used for the control and active surfaces, respectively. SH2 domain concentrations were the same as their K_d values shown in Table S2. The association phases of sensorgrams are shown here. It should be noted that for different proteins, absolute RU values do not necessarily reflect their relative affinity, because RU are relative values that depend on several factors, including the degree of non-specific binding of proteins to the control surface, membrane binding orientation of proteins, flow rate, instrumental parameters, and etc. To standardize our RU values and minimize the data variation caused by these factors, including different instrumental parameters of three separate SPR instruments used for measurements, the ‘relative response’ was used in lieu of absolute response values. Relative response was calculated by normalizing RU values against the maximal RU obtained for a particular protein under a given condition. Ultimate determination of relative affinity or lipid specificity would require K_d determination for a particular protein with different lipids or for different proteins.

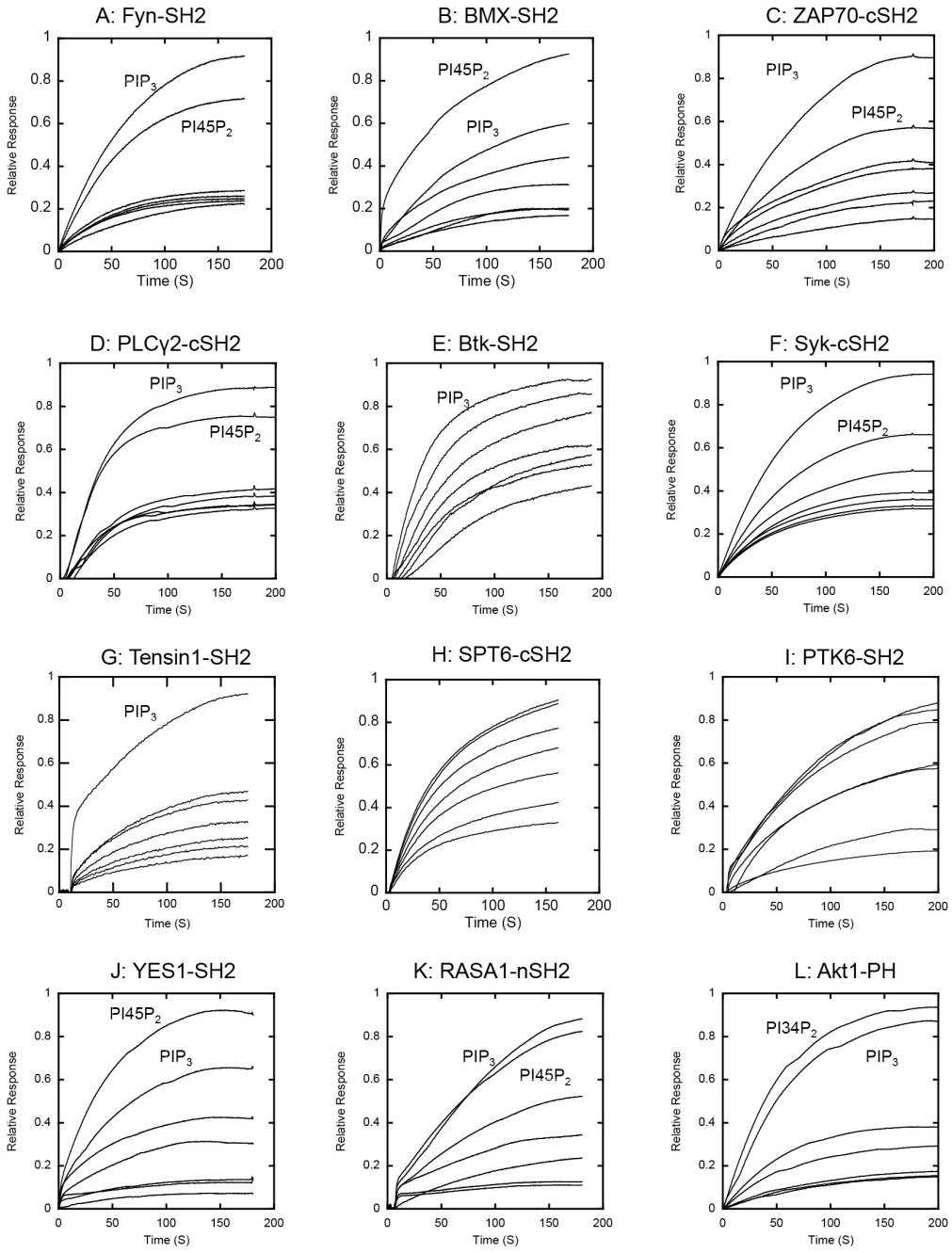
A: Fyn-SH2
PIP3
PI45P2
B: BMX-SH2
PI45P2
PIP3
C: ZAP70-cSH2
PIP3
PI45P2
D: PLCγ2-cSH2
PIP3
PI45P2
E: Btk-SH2
PIP3
F: Syk-cSH2
PIP3
PI45P2
G: Tensin1-SH2
PIP3
H: SPT6-cSH2
I: PTK6-SH2
J: YES1-SH2
PI45P2
PIP3
K: RASA1-nSH2
PIP3
PI45P2
L: Akt1-PH
PI34P2
PIP3
Relative Response
Time (S)

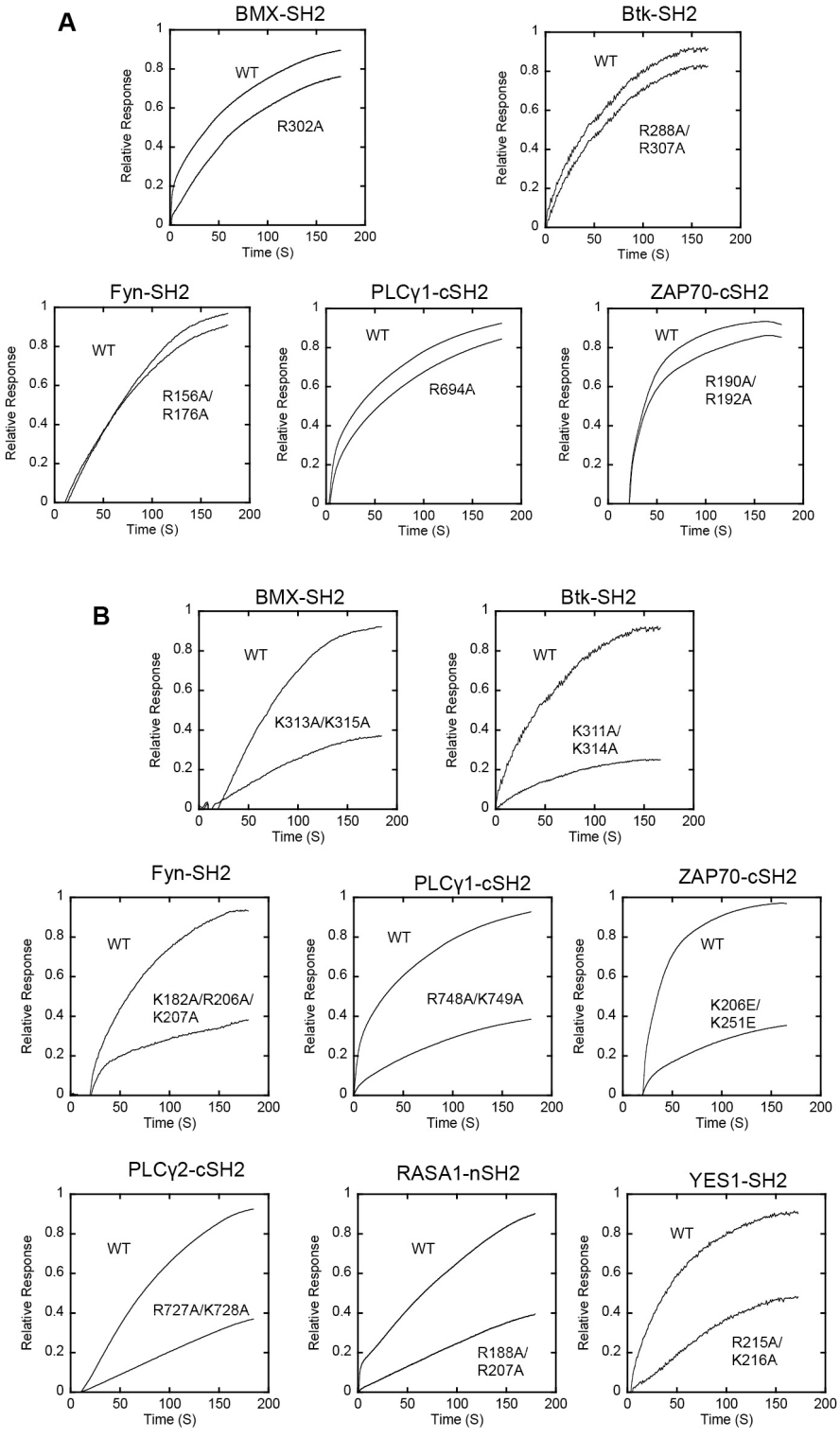

Fig. S2 (related to Fig. 2). Effect of mutating cationic residues in the pY pocket (A) and in alternate cationic patches (B) on membrane binding of SH2 domains. SPR measurements were performed in 20 mM Tris-HCl, pH 7.4, containing 0.16 M KCl. POPC vesicles and POPC/POPS/PtdInsP (77:20:3) vesicles were used for the control and active surfaces, respectively. SH2 domain concentrations were the same as their K_d values shown in Table S1. cSH2 indicates the C-terminal SH2 domain of tandem SH2 domains.

Fig. S3 (related to Fig. 3). Orthogonal functionality of lipid and peptide binding sites of SH2 domains and mutants.

(**A**) Binding of ZAP70-cSH2, Fyn-SH2 and PTK6-SH2 to pY peptides monitored by fluorescence anisotropy in the presence (square) and absence (circle) of 40 μM PM vesicles (POPC/POPE/POPS/POPI /cholesterol/PI45P_2 (12:35:22:8:22:1)). The peptide concentrations used varied from 5 nM to 5 μM depending on their K_d values. Notice that vesicles have no effect on peptide binding of all SH2 domains.

(**B**) Effect of pY peptides on membrane binding of ZAP70-cSH2, Fyn-SH2 and PTK6-SH2. The SH2 domains were allowed to interact with the PM mimetic vesicles before and after 30-min incubation with 100 μM peptides. SH2 domain concentrations were the same as their K_d values. The peptides have negligible effects on the membrane binding of SH2 domains, showing the orthogonality of lipid and peptide binding for these SH2 domains. Peptides used were: EIpYEE (PTK6-SH2), pYEEI (Fyn-SH2), and QLpYNEL (ZAP70-cSH2). cSH2 indicates the C-terminal SH2 domain of tandem SH2 domains.

(**C**) Model structures of ZAP70-cSH2 interacting with TCR-ζ and PI45P_2 in the PM. ZAP70-cSH2 (purple) and the TCR-ζ fragment containing a transmembrane segment (green) are shown in ribbon representation and PI45P_2 (brown) and other lipids in the PM are in stick representation. Notice that there is no steric overlap between the TCR-ζ molecule and PI45P_2 while ZAP70-cSH2 interacts with the PM containing these molecules. PM contains POPC, POPE, POPS, cholesterol, PI and PI45P_2 in a ratio of 12:35:22:22:8:1 that recapitulates the composition of inner PM of mammalian cells.

(**D**) PM vesicles do not interfere the binding of intact ZAP70 to phospho-TCR-ζ-ITAM. Bacterially expressed GST-TCR-ζ-ITAM was phosphorylated by Lck. 200 μg phospho-TCR-ζ-ITAM was incubated with 100 μg ZAP70 in the presence and the absence of 40 μM PM vesicles. Either 2.5 or 5 μg of phospho-TCR-ζ-ITAM in the incubation mixture was loaded onto the gel. The mixture was immunoblotted (IB) with ZAP70 and GST antibodies, respectively.

(**E**) Affinity of ZAP70-cSH2 WT (blue), K176E/K186E (orange), D184K (cyan), K206E/K251E (red), and R190A/R192A (green) for a pY-containing peptide (QL**pY**NEL) from the TCR-ζ ITAM was measured by fluorescence anisotropy analysis. ZAP70-cSH2 WT (K_d = 46 ± 7 nM), K176E/K186E (K_d = 48 ± 7 nM), D184K (K_d = 44 ± 10 nM), and K206E/K251E (K_d = 51 ± 8 nM) showed comparable affinity whereas R190A/R192A exhibited a ≈10-fold decrease in affinity (K_d = 440 ± 50 nM). The peptide concentrations used varied from 5 nM to 500 nM depending on the K_d values.

(**F**) Binding of intact ZAP70 WT, K176E/K186E, D184K, R190A/R192A, and K206E/K251E to the glutathione-Agarose resin-bound GST-TCR-ζ ITAM doubly Tyr-phosphorylated by Lck. 0, 2, 5, and 10 μg of ZAP70 proteins were incubated with ≈10 μg of GST-TCR-ζ ITAM. ZAP70 WT and GST alone were used as a control. The mixture was immunoblotted (IB) with ZAP70 and GST antibodies, respectively

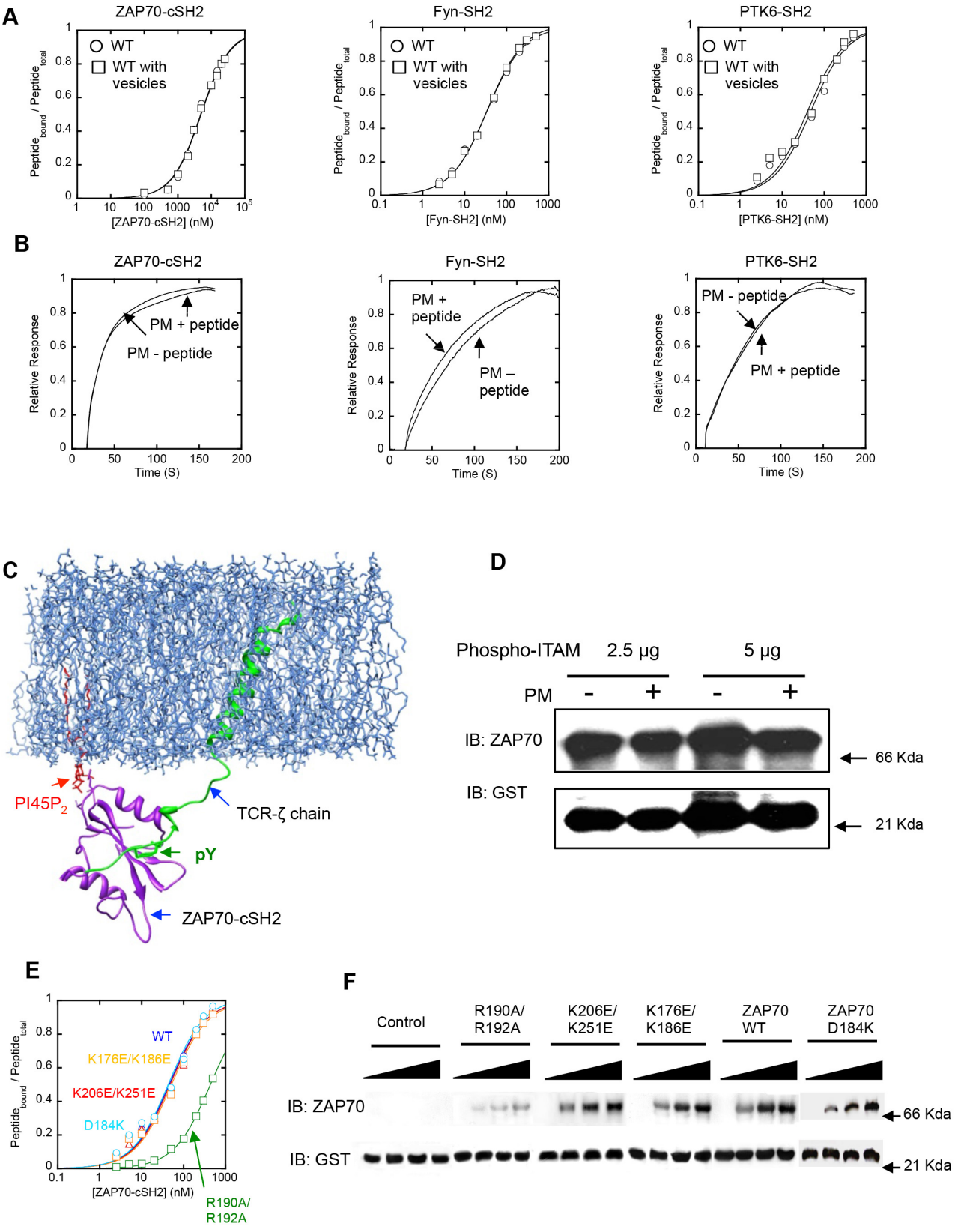
A
ZAP70-cSH2
WT
WT with vesicles
Peptide bound / Peptide total
[ZAP70-cSH2] (nM)
Fyn-SH2
[Fyn-SH2] (nM)
PTK6-SH2
[PTK6-SH2] (nM)
B
Relative Response
PM + peptide
PM - peptide
Time (S)
PM – peptide
C
PI45P2
TCR-ζ chain
pY
ZAP70-cSH2
D
Phospho-ITAM
2.5 µg
5 µg
PM
IB: ZAP70
66 Kda
IB: GST
21 Kda
E
WT
K176E/K186E
K206E/K251E
D184K
R190A/ R192A
F
Control
R190A/ R192A
K206E/ K251E
K176E/ K186E
ZAP70 WT
ZAP70 D184K

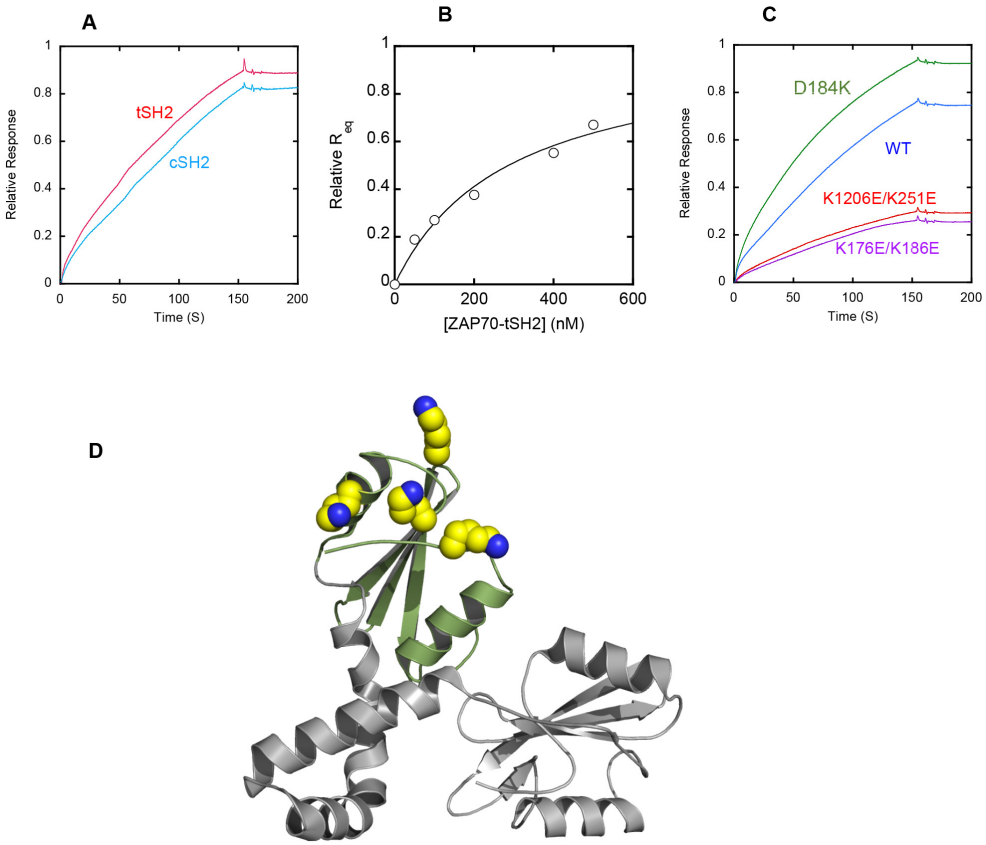

Fig. S4 (related to Fig. 3A and 4A). Lipid binding properties of ZAP70 tandem SH2 domains (ZAP70-tSH2) and mutants. (A) Kinetic SPR sensorgrams for ZAP70 cSH2 and tandem SH2 domains (tSH2). (B) Determination of K_d for ZAP70-tSH2-vesicle binding by equilibrium SPR analysis. The binding isotherm was generated from the R_{eq} (average of triplicate measurements) versus the concentration (P_0) of ZAP70-tSH2 plot. A solid line represents a theoretical curve constructed from K_d (= 290 ± 80 nM) values determined by nonlinear least squares analysis of the isotherm using the following equation: Relative R_{eq} = 1/(1 + K_d/P_0). (C) Kinetic SPR sensorgrams for ZAP70-tSH2 and its LOF and GOF mutants. Notice that these mutations had similar degrees of effects on cSH2 (see Fig 3A and 3B) and tSH2. SPR measurements were performed in 20 mM Tris-HCl (pH 7.4) containing 0.16 M KCl. POPC vesicles and POPC/POPS/PIP_3 (77:20:3) vesicles were used for the control and active surfaces, respectively. SH2 domain concentrations were 200 nM for all measurements. (D) The crystal structure of ZAP70-tSH2 (PDB ID: 2OQ1) demonstrating that the lipid binding residues (space-filling representation) of ZAP70-cSH2 (green) are fully exposed in ZAP70-tSH2. ZAP70-nSH2 and the connecting part are shown in gray. ZAP70-cSH2 is oriented as shown in Fig. 3A.

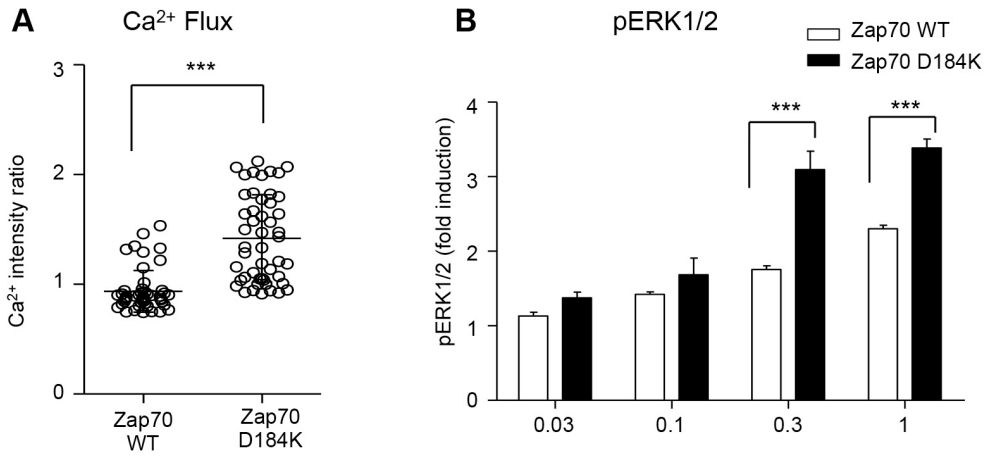

Fig. S5 (related to Fig. 4). TCR signaling activities of EGFP-tagged Zap70 WT and D184K mutant transduced into P116 cells. (A) Cells were labeled with Fura-2 AM and the calcium flux was monitored 3 min after OKT3 (0.05 μg/ml) treatment by microscopy. Each circle represents a single cell. *** $p < 0.001$ (Student's t-test). Notice that the OKT3 concentration used here is 6-times lower than that used for Fig. 4D. (B) Cells were stimulated with indicated doses of OKT3 for 5 min and the levels of pERK1/2 were measured by intracellular staining and flow cytometry. To compensate for the differences in expression levels of WT and the GOF mutant, cells expressing similar levels of EGFP-tagged proteins were gated and used for quantitative analysis.

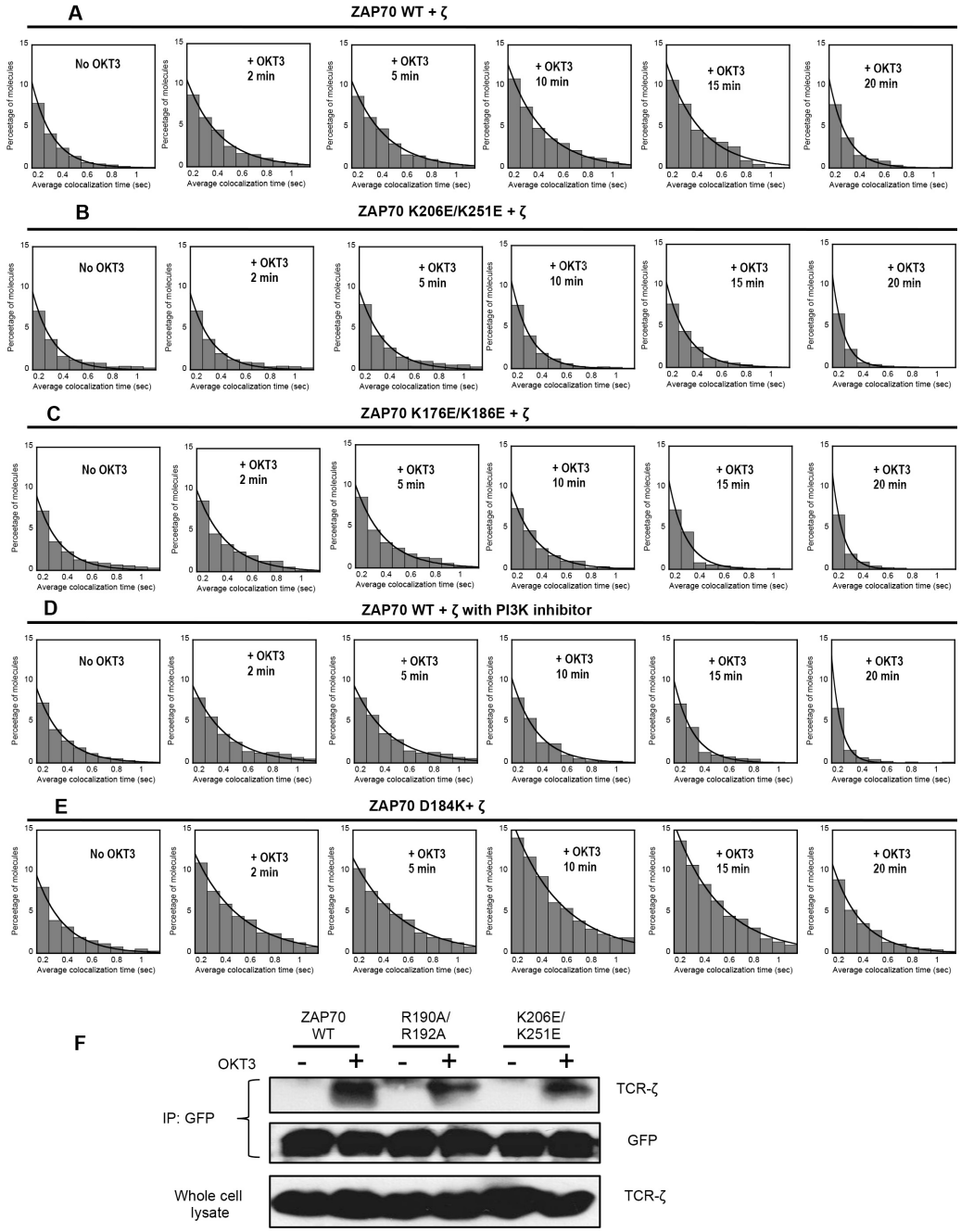

Fig. S6 (related to Fig. 6). Effect of lipids on cellular ZAP70-TCR-ζ interaction. (A)-(E) Time-courses of dynamic colocalization of SNAP-TMR-TCR-ζ and EGFP-ZAP70 (WT and mutants). The histograms display percentages of TCR-ζ molecules spending a given colocalzation time (>0.2 sec) with ZAP70 on the PM of P116 cells. For PI3K inhibition (-PIP_3), cells were pre-treated with 50 μM LY294002 for 1 h before OKT3 stimulation. 10 μg/ml OKT3 was used in all experiments. Error bars indicate S.D. (*n* = 50-100). (F) Coimmunoprecipitation of ZAP70 WT and mutants with TCR-ζ. P116 cells stably transfected with GFP-ZAP70 WT, R190A/R192A (pY site mutant) and K206E/K251E (non-specific lipid binding LOF mutant) were stimulated with 10 μg/ml OKT3 for 5 min before harvesting. The lysates were immuno-precipitated (IP) with the GFP antibody and binding to TCR-ζ was then detected by the TCR-ζ-specific antibody. Co-IP showed reduced binding of TCR-ζ with GFP-tagged ZAP70 mutants, R190A/R192A and K206E/K251E, compared to GFP-ZAP70 WT. The GFP bands of GFP-immunoprecipitated proteins and the TCR-ζ bands in the whole cell lysate were shown to demonstrate similar expression levels of ZAP70 proteins and TCR-ζ, respectively, in these cells.

A

SH2 domains	PTK6-SH2 WT	PTK6-SH2 R85A/R105A	PTK6-SH2 R131A/R136A
K_d (nM)	150 ± 50	200 ± 70	700 ± 150

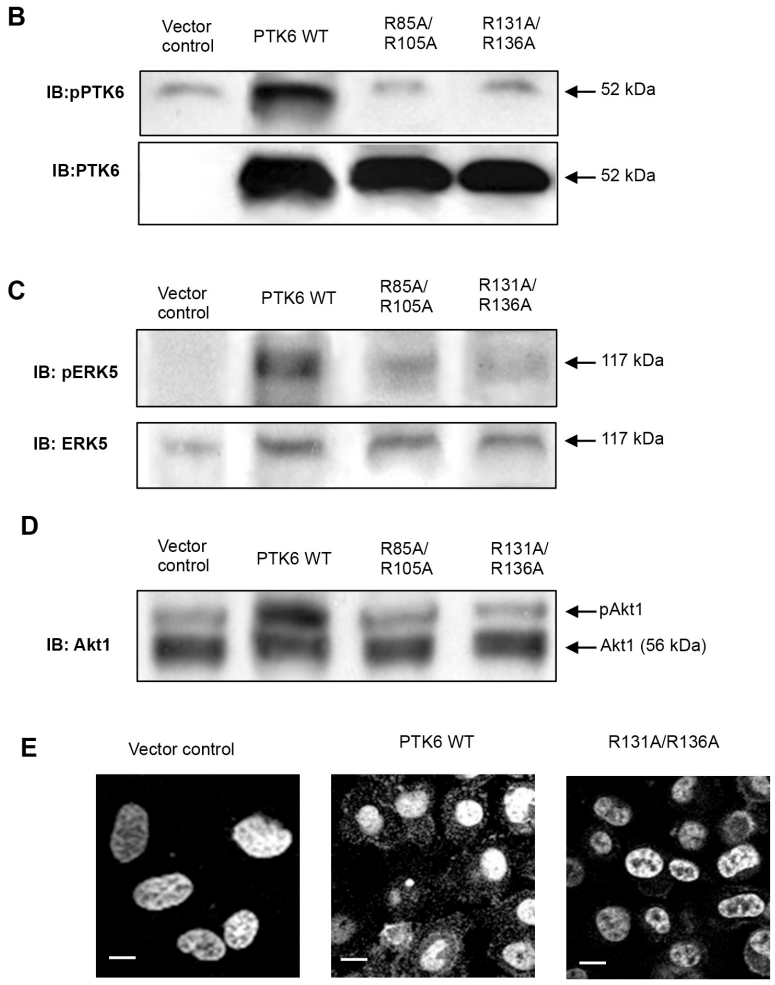

Fig. S7 (related to Fig. 3). Roles of lipids in cell signaling activities of PTK6. (A) Relative affinity of PTK6-SH2 WT and mutants determined by SPR analysis using PM-mimetic vesicles. The pY site mutant (R85A/K105A) has similar PM affinity to WT whereas the ACP site mutant (R131A/R136A) has ≈5-fold lower affinity. (B) Autophosphorylation of Myc-tagged PTK6 WT and mutants transiently expressed in HEK293 cells. (C) Effect of PTK6 WT and mutants transiently expressed in HEK293 cells on phosphorylation of endogenous ERK5. (D) Effect of PTK6 WT and mutants transiently expressed in HEK293 cells on phosphorylation of endogenous Akt1. (E) Subcellular localization of PTK6 WT and R131A/R136A transiently expressed in HEK293 cells. Immunostaining on fixed cells were performed using the antibody against PTK-pY342. Nuclei were stained with Hoechst 33342 dye to visualize cells. Scale bars indicate 5 μm. Notice that PTK6 WT shows strong PM localization of pY342 species whereas R131A/R136A has a negligible degree of pY342 and PM localization. HEK293 cells were serum-starved for 48 h and then activated with fetal bovine serum for 1 h. The Western blotting was performed with the antibody specific for each protein.

SUPPLEMENTAL TABLES

Table S1 (related to Table 1).

Effects of EGFP on Lipid Binding Properties of SH2 Domains

SH2 domains	Tag[a]	K_d (nM) for PM[b]
BRK(PTK6)-SH2	No tag	105 ± 2
	C-EGFP	100 ± 2
Tensin2-SH2	No tag	230 ± 100
	C-EGFP	200 ± 67
SYK-cSH2[c]	No tag	NM[e]
	N-EGFP	210 ± 9
	C-EGFP	230 ± 44
PLCγ1-cSH2[d]	No tag	NM[e]
	N-EGFP	290 ± 16
	C-EGFP	1300 ± 120

[a]N-terminal or C-terminal EGFP tag.
[b]Mean ± S.D. from triplicate equilibrium SPR measurements using PM mimetic vesicles (POPC/POPE/POPS/PI/cholesterol/PI4,5P_2 (12:35:22:8:22:1)).
[c]For most SH2 domains, N-terminal and C-terminal EGFP tags have essentially the same minimal effects on their membrane binding. The C-terminal EGFP tag was selected over the N-terminal one because the former tends to stabilize the SH2 domain better than the latter. cSH2 indicates the C-terminal SH2 domain of the tandem SH2 domains.
[d]For some SH2 domains, we employed the N-terminal EGFP tag because the C-terminal EGFP tag interferes with their lipid binding. cSH2 indicates the C-terminal SH2 domain of the tandem SH2 domains.
[e]Not measured

Table S2. (related to Fig. 2)

Analysis of PtdIns*P* binding cavities of SH2 and PH domains

	ZAP70-cSH2	BMX-SH2	BTK-PH[a]
PtdInsP specificity	PIP_3 > $PI45P_2$ > others	$PI45P_2$ > PIP_3 > others	PIP_3 >> others
Area (Å^2)	70.3	43.1	119.3
Average depth (Å)	3.9	3.4	3.7
Max depth (Å)	6.2	4.9	6

[a]From PDB ID: 1B55

Table S3. (related to Fig. 4 and Table 1)

Lipid Binding Properties of ZAP70 SH2 Domain Mutants

Proteins	[e]K_d (nM) for POPC/POPS/PIP_3 (77:20:3) vesicles
[a]ZAP70-[b]cSH2 WT	200 ± 10
[a]ZAP70-[b]cSH2 K176E/K186E	950 ± 150
[a]ZAP70-[b]cSH2 K206E/K251E	760 ± 100
[a]ZAP70-[b]cSH2 D184K	60 ± 20
[a]ZAP70-[c]tSH2 WT	290 ± 80
ZAP70 [d]FL WT	240 ± 60
ZAP70 [d]FL K176E/K186E	760 ± 200
ZAP70 [d]FL K206E/K251E	500 ± 150

[a]EGFP-fusion proteins
[b]cSH2 indicates the C-terminal SH2 domain of the tandem SH2 domains.
[c]tSH2 indicates the tandem SH2 domains (residues 1-263).
[d]Full-length proteins
[e]Mean ± S.D. from triplicate equilibrium SPR measurements using POPC/POPS/PIP_3 (77:20:3) vesicles.

MOVIE LEGENDS

Movie S1. (related to Fig. 5A) Simultaneous single molecule tracking of EGFP-ZAP70 WT and SNAP-TMR-TCR-ζ in a P116 cell before OKT3 stimulation. Green, red, and yellow dots show individual ZAP70 and individual TCR-ζ molecules, and co-localized molecules, respectively.

Movie S2. (related to Fig. 5A) Simultaneous single molecule tracking of EGFP-ZAP70 WT and SNAP-TMR-TCR-ζ in a P116 cell cell 5 min after OKT3 stimulation. Green, red, and yellow dots show individual ZAP70 and individual TCR-ζ molecules, and co-localized molecules, respectively.

Movie S3. (related to Fig. 5B) Simultaneous single molecule tracking of EGFP-ZAP70 K206E/K251E and SNAP-TMR-TCR-ζ in a P116 cell cell before OKT3 stimulation. Green, red, and yellow dots show individual ZAP70 and individual TCR-ζ molecules, and co-localized molecules, respectively.

Movie S4. (related to Fig. 5B) Simultaneous single molecule tracking of EGFP-ZAP70 K206E/K251E and SNAP-TMR-TCR-ζ in a P116 cell cell 5 min after OKT3 stimulation. Green, red, and yellow dots show individual ZAP70 and individual TCR-ζ molecules, and co-localized molecules, respectively.

EXTENDED EXPERIMENTAL PROCEDURES

Materials

1-Palmitoyl-2-oleoyl-*sn*-glycero-3-phosphocholine (POPC), 1-palmitoyl-2-oleoyl-*sn*-glycero-3-phosphoethanolamine (POPE), 1-palmitoyl-2-oleoyl-*sn*-glycero-3-phosphoserine (POPS), cholesterol, liver phosphoinositol (PI) were purchased from Avanti Polar Lipids. 1,2-dipalmitoyl derivatives of phosphatidylinositol-4,5-bisphosphate ($PI45P_2$), phosphatidylinositol-3,4,5-trisphosphate (PIP_3), phosphatidylinositol-3,4-bisphosphate ($PI34P_2$), phosphatidylinositol-3,5-bisphosphate ($PI35P_2$), phosphatidylinositol-3-monophosphate (PI3P), phosphatidylinositol-4-monophosphate (PI4P), phosphatidylinositol-5-monophosphate (PI5P) were from Cayman Chemical Co. The human anti-CD3 antibody, OKT3, was purchased from Bio X cell, and anti-GFP antibody and anti-actin antibody were from Santa Cruz and Bethyl laboratories, respectively. Rabbit Anti-GFP was purchased from BD Bioscience and Mouse anti-TCR-ζ (6B10.2) was purchased from Santa Cruz Biotech. All other antibodies were from Cell Signaling Technologies.

DNA Constructs

cDNAs of human SH2 domains were isolated from human SH2 domain library by polymerase chain reaction (PCR) and subcloned into a pRsetB vector with the EGFP epitope at the C-terminus or the N-terminus. cDNA of the full length human ZAP70 was subcloned to pET30a(+) vector. Human full-length CD4 (a.a. 1-458) and human full-length TCR-ζ (CD247) (a.a. 1-164) were cloned to the pSNAPf vector (New England Biolab) using *Kpn*I/*Xho*I and *Eco*RI/*Eco*RV sites, respectively.

Protein Expression and Purification

Since many SH2 domains are not stably expressed in *Escherichia coli*, we expressed them as enhanced green fluorescence protein (EGFP)-fusion proteins, which significantly improved the protein expression yield for most SH2 domains without affecting their membrane binding properties. For most SH2 domains, N-terminal and C-terminal EGFP tags have essentially the same effect. The C-terminal EGFP tag was selected over the N-terminal one because the former tends to stabilize the SH2 domain better than the latter. For some SH2 domains, we employed the N-terminal EGFP tag because the C-terminal EGFP tag interferes with their lipid binding. All EGFP-tagged SH2 domains and full-length proteins were expressed as His_6-tagged proteins in *E. coli* BL21 (DE3) pLysS (Novagen). Cells were cultured to an OD_{600} of ~0.6 and protein expression was induced by adding 0.5-1 mM isopropyl-β-D-1-thiogalactopyranoside at 16°C for 12 h. The transformed cells were harvested by centrifugation at 4°C and cell pellets were resuspended in the lysis buffer (50 mM Tris-HCl, pH 7.9, 0.3 M NaCl, 10 mM imidazole, 10% glycerol, 1 mM 4-(2-aminoethyl)benzenesulfonyl fluoride), and lysed by sonication. The His-tagged proteins were purified using the Ni-NTA-Agarose resin (Qiagen). Eluted proteins were further treated on a PD-10 desalting column (GE Healthcare) equilibrated with 20 mM Tris-HCl pH 7.4, 0.16 M NaCl. Proteins were quantified by the Braford assay (Bio-Rad).

Lipid Vesicles Preparation and SPR Analysis

PM-mimetic vesicles were prepared by mixing POPC, POPE, POPS, cholesterol, PI, and $PI45P_2$ in a molar ratio of 12:35:22:22:8:1. Large unilamellar vesicles were prepared using a microextruder (Avanti Polar Lipids) with a 100 nm polycarbonate filter. All SPR measurements were performed at 23°C using a lipid-coated L1 chip in the BIACORE X and T100 systems as described (Stahelin and Cho, 2001). 20 mM Tris-HCl, pH 7.4, containing 0.16 M NaCl was used as the running buffer while PM-mimetic

vesicles and POPC (or POPC/POPS (8:2)) vesicles were coated on the active surface and the control surface, respectively. Vesicles were injected at 5 μl/min onto the corresponding sensor chip surfaces to yield the identical resonance units (RU), ensuring the equal concentration of the coated lipids. Equilibrium measurements were performed at a flow rate of 5 μl/min, which allowed enough time for the *R* values of the association phase to reach near equilibrium levels (R_{eq}) (Ananthanarayanan et al., 2003). Each sensorgram was background-corrected by subtracting the control surface response from the active surface response. A minimum of 5 different protein concentrations were injected to collect a set of R_{eq} values that were plotted against the protein concentrations (P_o). An apparent dissociation constant (K_d) was then determined by nonlinear least squares analysis of the binding isotherm using the equation, $R_{eq} = R_{max} / (1 + K_d/P_o)$ where R_{max} indicates the maximal R_{eq} value (Cho et al., 2001). Since the concentration of lipids coated on the sensor chip cannot be accurately determined, K_d is defined as P_o yielding half-maximal binding with a fixed lipid concentration. Each measurement was repeated at least three times to determine average and standard deviation values. For kinetic measurements, the flow rate was maintained at 20-30 μl/min. Relative response (in the scale of 0-1) was calculated by dividing RU values by the maximal RU obtained for a particular protein under a given condition. Relative response was used for most figures to standardize our RU values and minimize data variation caused by experimental factors, most notably different instrumental parameters of three separate SPR instruments used for measurements.

Stable Cell Line Preparation:

A Jurkat cell line derivative, P116 (CRL-2676), was from ATCC and cultured in RPMI 1640 containing 5% fetal bovine serum. ZAP70 WT and mutants were stably expressed in P116 by retroviral gene transduction. A retroviral construct, pLEGFP-N1-hZap70, was cloned by PCR and point mutations were introduced by site-directed mutagenesis. Retrovirus preparation and transduction were performed as previously described (Kim et al., 2013).

Single Cell Calcium Imaging

Changes in the intracellular calcium levels were assessed by microscopy. Cells were loaded with ratiometric calcium indicator Fura-2 AM (2 μg/ml, Life Technologies) in phenol red-free DMEM media containing 0.5% FBS for 30 min at 37°C, washed, and plated to a poly-L-lysine-coated culture plate for imaging. The changes in the fluorescence emission of calcium-bound and unbound form of Fura-2 were captured using an OLYMPUS fluorescence microscope with a Hamamatsu ImagEM electron multiplier CCD camera. The fluorescence emission ratio of individual cells was analyzed using MetaFluor (Molecular devices) and Prism (GraphPad) software.

Tyrosine Phosphorylation Assay

Cells expressing either WT or mutant GFP-ZAP70 were stimulated with OKT3 (3 μg/ml) at 37°C for indicated time. Cells were then immediately lysed by addition of ice-cold radioimmunoprecipitation assay buffer supplemented with a protease inhibitor mixture and a protein phosphatase inhibitor mixture. The proteins were separated by sodium dodecyl sulfate polyacrylamide gel electrophoresis, transferred to a nitrocellulose membrane, and probed with antibodies against pLAT (Y191), pPLCγ1 (Y783), pERK1/2 (T202/Y204), pZAP70 (Y493) and β-actin. The chemiluminescence was detected with ImageQuant LAS 4000 (GE Healthcare).

IL-2 ELISA

Cells were added to 96 well plate (2×10^6 cells per well) coated with OKT3 and anti-CD28 antibodies

and incubated for 24 h. The levels of IL-2 in culture supernatants were measured by sandwich ELISA (eBioscience).

Rapamycin-inducible $PI45P_2$ depletion and PIP_3 enrichment

The $PI45P_2$ depletion was performed according to a reported procedure (Inoue et al., 2005; Varnai et al., 2006). Our modified $PI45P_2$ depletion system consists of the Lyn-based PM-anchored FKBP12-rapamycin binding (FRB) domain of mTOR (Lyn-FRB) and the FK506-binding protein-12-yeast inositol polyphosphate 5-phosphatase domain fusion protein (FKBP-Inp) whose heterodimerization is triggered by rapamycin (Yoon et al., 2011). HeLa cells were seeded into cell plates and then incubated with DMEM containing 10% (v/v) FBS, 1% penicillin and streptomycin at 37^0C with 5% CO_2 for 24 hours. The cells were co-transfected with PM-FRB, FB-Inp, and mCherry-tagged SH2 domain plasmids in a 2:2:1 ratio for 5 h (0.5 μg of total DNA/well) in the presence of Lipofectamine 2000 (Invitrogen) in DMEM without FBS. Cells were incubated with DMEM containing 10% FBS overnight. Before imaging, the medium was replaced by clear DMEM and then images of cells were taken to identify cells expressing corresponding proteins. After initial imaging, the PM translocation of mCherry-ZAP70-cSH2 WT and mutants was monitored in the presence of 2.5 μM rapamycin analog, A/C Heterodimerizer (Clontech). The PIP_3 enhancement system consists of PM-anchored Lyn-FRB and YF-iSH (YFP-tagged FKBP with an inter SH2 domain (420–615) of p85β (gene accession number: BC006796)) (Inoue and Meyer, 2008). PIP_3 enhancement was also triggered by A/C Heterodimerizer. To demonstrate the robustness of these $PI45P_2$ depletion and PIP3 enrichment systems, we monitored the PM localization of microinjected $PI45P_2$ (Yoon et al., 2011) and PIP_3 (Liu et al., 2014) sensors after stimulation with A/C Heterodimerizer.

SH2-Peptide Binding Assay by Fluorescence Anisotropy

Fluorescein-6-aminohexanoyl (F-Ahx)-labeled peptides used for binding studies are as follows: F-Ahx-pYEEI (Fyn-SH2), F-Ahx-QLpYNEL (ZAP70-cSH2), and F-Ahx-EIpYEE (PTK6-SH2). The peptide was dissolved in 20 mM Tris buffer, pH 7.4, containing 160 mM NaCl, and 5% dimethylsulfoxide. To each well of a 96-flat bottom black polystyrol plate was added 100 μl solution containing each peptide (5 nM) and SH2 domain (2.5 nM to 25 μM) with or without 150 μM PM vesicles. After 30-min incubation, the plate was inserted into BioTek Synergy Neo microplate reader and the fluorescence anisotropy (r) was measured with excitation and emission wavelengths set at 485 and 535 nm, respectively. Since $P_o >> Pep_o$ under our conditions, the K_d for the SH2 domain-peptide binding was determined by the non-linear least-squares analysis of the binding isotherm using the equation:

$$Pep_{bound} / Pep_o = \Delta r / \Delta r_{max} = \frac{1}{1 + K_d/P_o}$$

where Pep_{bound}, Pep_o, and P_o indicate the concentration of bound peptide, total peptide and total SH2 domain, respectively, and Δr and Δr_{max} are the anisotropy change for each P_o and the maximal Δr, respectively.

ZAP70-ITAM binding assay

The ITAM sequence from the human ζ chain (residue number 52-93) was cloned to the pGEX 4T-1 vector. The glutathione-S-transferase (GST)-conjugated ITAM plasmid was transformed into *Escherichia coli* BL21 (DE3)pLysS (Novagen). The empty pGEX 4T-1 vector was used as a control. Cells were cultured to an OD_{600} of ~0.6 and protein expression was induced by adding 0.5-1 mM isopropyl-β-D-1-thiogalactopyranoside at room temperature for ~14 h. Cells were harvested by centrifugation at 4^oC and resuspended in the lysis buffer (50 mM Tris-HCl, pH 7.9, 0.3 M NaCl, 10% glycerol, 1 mM 4-(2-aminoethyl)benzenesulfonyl fluoride, 1 mM dithiothreitol), and lysed by sonication. The proteins were immobilized on a glutathione-Agarose resin and washed thoroughly with 20 mM

Tris-HCl, 160 mM NaCl, pH 7.4. For the *in vitro* phosphorylation, the ITAM-containing resin was placed in the reaction buffer (30 mM Tris-HCl, 20 mM $MgCl_2$, 2 mM ATP, pH 7.5) and ~0.1 mg/ml of recombinant Lck was added to the solution. After incubation at room temperature for 45 min, the reaction was quenched by adding 200 mM EDTA. Double phosphorylation of the ITAM was confirmed by mass spectrometry of the protein eluted from the resin using the unphosphorylated GST-ITAM as a standard. The resin was extensively washed with 20 mM Tris-HCl, 160 mM NaCl, pH 7.4 to remove excess reagents. Then 40 μg of resins containing GST-ITAM or GST alone were mixed with 0-10 μg of recombinant human ZAP70. The mixtures were incubated at room temperature for 30 min and the resins were washed three times with 20 mM Tris-HCl, 160 mM NaCl, pH 7.4 by centrifugation. The resins were then boiled in a gel loading buffer. The supernatant was loaded on to a sodium dodecylsulfate-polyacrylamide gel and separated by electrophoresis. Western blotting was performed using antibodies for ZAP70 and GST and the goat anti-rabbit-horse radish peroxidase secondary antibody. ZAP70-ITAM binding was also performed in the presence of 40 μM PM vesicles to check the effect of lipids on ZAP70-ITAM binding.

Single Molecule Tracking by Total Internal Reflection Fluorescence Microscopy

Simultaneous single molecule imaging of two proteins was performed in Jurkat cells using a total internal reflection fluorescence microscope custom-built on the Olympus IX71 microscope base as described previously (Sheng et al., 2012). P116 cells stably expressing EGFP-ZAP70 WT (or mutants) were transiently transfected with SNAP®-tagged TCR-ζ. Cells were labeled with SNAP-Cell® tetramethylrhodamine (TMR)-Star® (New England Biolabs), washed, and stimulated with OKT3 to simultaneously track ZAP70 and the activated CD3 complex. To see the effect of PIP_3 depletion on interaction between ZAP70 WT and TCR-ζ, cells were pre-treated with 50 μM LY294002 for 1 h before OKT3 stimulation. Two DPSS laser sources (488 and 561 nm, Excelsior, Spectra-Physics) were used and the fluorescence signal from the sample was split into two channels, passed through emission filters (510BP20, Omega and D630/30, Chroma), and projected onto two Andor iXon 897 EM-CCD cameras. The images were spatially corrected following the algorithm described previously (Koyama-Honda et al., 2005). All particle tracking, data analysis and image processing were carried out with in-house programs written in MATLAB. Co-localization analysis of two molecules was performed with a fixed threshold criterion (i.e., <400 nm) for co-localization (Koyama-Honda et al., 2005). The same size of PM surface was analyzed for each data. The percentage TCR-ζ molecules spending a given colocalzation time (>0.2 sec) with ZAP70 on the PM of P116 cells was calculated from the total number of TCR-ζ molecules and displayed as a histogram. Data were fit into a single exponential decay equation (i.e., $P = P_o e^{-kt}$) to determine the dissociation rate constant (k) values by non-linear least-squares analysis and the half-life values of co-localization were calculated as $ln2/k$. 50-100 images were analyzed for each data point.

Co-immunoprecipitation of ZAP70 and TCR-ζ

P116 cells stably transfected with GFP-ZAP70 WT, R190A/R192A, and K206E/K251E were stimulated with OKT3 (10 μg/ml) for 5 min. Cells were harvested and proteins were immunoprecipitated with the GFP antibody and protein A agarose beads. The complex was loaded on to a sodium dodecylsulfate-polyacrylamide gel and separated by electrophoresis. Western blotting was performed using antibodies for GFP and TCR-ζ. TCR-ζ in the whole cell lysate was used as a loading control.

PTK6 Assays

Human full-length PTK6 gene was subcloned into pcDNA3 vector with the N-terminal Myc tag. HEK293 cells were transfected by either PTK6-pcDNA3 (WT or mutants) or empty pcDNA3 vector using Lipofactamine 2000. For the fractionation assay, the cells were cultured in the serum-containing medium and incubated at 37^{o}C with 5% CO_2 for 14 h after transfection. Then fractionation was performed using the ProteoExtract kit from Calbiochem according to the manufacturer's protocol. Immunoblotting was performed using anti-E-Cadherin (Millipore), anti-GAPDH (Millipore), anti-SP1 (Cell Signaling), anti-PTK6 pY304 (Cell Signaling) and anti-Myc (Millipore) antibodies, together with the goat anti-rabbit horseradish peroxidase conjugated secondary antibody (Millipore). For the functional assay, after transfection of the plasmids mentioned above, the cells were starved for 48 h in a serum-free medium. Then, 20% of fetal bovine serum was added to each well to activate cells for 10 min. After the stimulation, the cells were immediately harvested and lysed. For immunoblotting, anti-Akt (Cell Signaling) and anti-Erk5/anti-phospho-ERK5 antibodies (Cell Signaling), and the goat anti-rabbit horseradish peroxidase conjugated secondary antibody were used.

Models of SH2 Domains

The models for SH2 domains, structures of which were not available in the PDB, were created with Modeller 9.9 (Sali and Blundell, 1993). The templates were searched with Psi-blast (Altschul et al., 1997) against the sequence database of PDB. The quality of the models was assessed in terms of pG score – the posterior probability that the model has a correct 3D conformation, given its normalized z-score (obtained using the program Prosa II (Sippl, 1993)) and length. All models of SH2 domains shown in this study have a pG score of 1.00.

Electrostatic and Cavity Analysis

The PDB files were prepared for further calculations using PDB2PQR interface (Dolinsky et al., 2007; Dolinsky et al., 2004). We used PROPKA (Li et al., 2005; Rostkowski et al., 2011) to predict protonation states of protein residues. DelPhi (Rocchia et al., 2001) was used for assigning electrostatic potentials to the atoms of the structures. Only linear DelPhi iterations were run. Both PROPKA and Delphi used CHARMM force field (MacKerell et al., 1998). The calculated potentials were loaded into GRASP2 (Petrey and Honig, 2003) for subsequent visualization. Identifying protein cavities and computing cavity attributes was performed with Screen (Nayal and Honig, 2006). The input files with grid electrostatic potentials were generated with DelPhi (Rocchia et al., 2001).

Docking

Docking of the lipids to the structure of SH2 domains was performed with the DOCK program of the package DOCK 6 (Lorber and Shoichet, 1998; Wei et al., 2002). The spheres representing the binding site were selected within 7 Å from the side-chains of the residues shown to be important for the lipid binding. The ligand was allowed to be flexible during the orientation step. The topmost pose generated by DOCK run was rescored using Amber score program, which allows both the ligand and the active site of the receptor to be flexible (Graves et al., 2008).

Multiple Sequence Alignments

Multiple sequence alignments were generated with CLUSTAL 2.0.10 (Larkin et al., 2007).

Modeling of the complex of membrane bilayer with ZAP70-cSH2 and CD3 zeta chain

The membrane bilayer was built with Membrane Builder program (Call et al., 2006) of CHARMM_GUI

(Jo et al., 2008). The initial bilayer measured 10x10 lipids and contained POPC, POPE, POPS, cholesterol, PI and $PI45P_2$ in a ratio of 12:35:22:22:8:1 (phosphoinositides were present only in the inner layer of the membrane). To dock c-SH2 domain of ZAP70 to the membrane, the complex of ZAP70-cSH2 with the headgroup of $PI45P_2$ and the cognate peptide of TCR ζ chain (see above for the modeling of the complex) was superimposed on the headgroup of $PI45P_2$ in the membrane. The superimposition was performed with Chimera program (Pettersen et al., 2004). The initial coordinates of the transmembrane domain of TCR ζ chain were taken from the solution NMR structure of TCR ζ dimer (PDB ID: 2HAC) (Soto et al., 2008). The transmembrane domain was inserted into the bilayer using Chimera. The peptide sequence between the transmembrane domain and the cognate peptide of ZAP70 was modelled with loopy program (Wu et al., 2014; Xiang et al., 2002).

NMR Data Acquisition and Processing

The ^{1}H-, ^{13}C-, ^{15}N-HSQC experiments were recorded at 600- and 800-MHz on Bruker Avance spectrometers at 20ºC. The samples contained 0.1 mM of ^{13}C- or ^{15}N-labeled Fyn-SH2 and PTK6-SH2, respectively, in 25 mM potassium phosphate, 2 mM dithiothreitol and 5% deuterium oxide (pH 6.0). D-myo-inositol-(1,3,4,5)-tetrakisphosphate (IP_4) was titrated to a final concentration of 1 mM. All NMR data were processed with NMRpipe (Delaglio et al., 1995) and analyzed with CARA. The chemical shift perturbations (CSPs) upon addition of IP_4 were calculated from ^{1}H, ^{13}C, and ^{15}N chemical shifts using a weighted averaging scheme previous described (Farmer et al., 1996; Grzesiek et al., 1996; Pellecchia et al., 2000). Missing shifts are indicative of either unavailable experimental data, owing to peak overlap or a residue position occupied by a proline.

SUPPLEMENTAL REFERENCES

Altschul, S.F., Madden, T.L., Schaffer, A.A., Zhang, J., Zhang, Z., Miller, W., and Lipman, D.J. (1997). Gapped BLAST and PSI-BLAST: a new generation of protein database search programs. Nucleic Acids Res. *25*, 3389-3402.

Ananthanarayanan, B., Stahelin, R.V., Digman, M.A., and Cho, W. (2003). Activation mechanisms of conventional protein kinase C isoforms are determined by the ligand affinity and conformational flexibility of their C1 domains. J. Biol. Chem. *278*, 46886-46894.

Call, M.E., Schnell, J.R., Xu, C., Lutz, R.A., Chou, J.J., and Wucherpfennig, K.W. (2006). The structure of the zetazeta transmembrane dimer reveals features essential for its assembly with the T cell receptor. Cell *127*, 355-368.

Cho, W., Bittova, L., and Stahelin, R.V. (2001). Membrane binding assays for peripheral proteins. Anal. Biochem. *296*, 153-161.

Delaglio, F., Grzesiek, S., Vuister, G.W., Zhu, G., Pfeifer, J., and Bax, A. (1995). NMRPipe: a multidimensional spectral processing system based on UNIX pipes. J. Biomol. NMR *6*, 277-293.

Dolinsky, T.J., Czodrowski, P., Li, H., Nielsen, J.E., Jensen, J.H., Klebe, G., and Baker, N.A. (2007). PDB2PQR: expanding and upgrading automated preparation of biomolecular structures for molecular simulations. Nucleic Acids Res *35*, W522-525.

Dolinsky, T.J., Nielsen, J.E., McCammon, J.A., and Baker, N.A. (2004). PDB2PQR: an automated pipeline for the setup of Poisson-Boltzmann electrostatics calculations. Nucleic Acids Res. *32*, W665-667.

Farmer, B.T., 2nd, Constantine, K.L., Goldfarb, V., Friedrichs, M.S., Wittekind, M., Yanchunas, J., Jr., Robertson, J.G., and Mueller, L. (1996). Localizing the NADP+ binding site on the MurB enzyme by NMR. Nat. Struct. Biol. *3*, 995-997.

Graves, A.P., Shivakumar, D.M., Boyce, S.E., Jacobson, M.P., Case, D.A., and Shoichet, B.K. (2008). Rescoring docking hit lists for model cavity sites: predictions and experimental testing. J. Mol. Biol. *377*, 914-934.

Grzesiek, S., Stahl, S.J., Wingfield, P.T., and Bax, A. (1996). The CD4 determinant for downregulation by HIV-1 Nef directly binds to Nef. Mapping of the Nef binding surface by NMR. Biochemistry *35*, 10256-10261.

Inoue, T., Heo, W.D., Grimley, J.S., Wandless, T.J., and Meyer, T. (2005). An inducible translocation strategy to rapidly activate and inhibit small GTPase signaling pathways. Nat. Methods *2*, 415-418.

Inoue, T., and Meyer, T. (2008). Synthetic activation of endogenous PI3K and Rac identifies an AND-gate switch for cell polarization and migration. PLoS One *3*, e3068.

Jo, S., Kim, T., Iyer, V.G., and Im, W. (2008). CHARMM-GUI: a web-based graphical user interface for CHARMM. J. Comput. Chem. *29*, 1859-1865.

Kim, J., Huh, J., Hwang, M., Kwon, E.H., Jung, D.J., Brinkmann, M.M., Jang, M.H., Ploegh, H.L., and Kim, Y.M. (2013). Acidic amino acid residues in the juxtamembrane region of the nucleotide-sensing TLRs are important for UNC93B1 binding and signaling. J. Immunol. *190*, 5287-5295.

Koyama-Honda, I., Ritchie, K., Fujiwara, T., Iino, R., Murakoshi, H., Kasai, R.S., and Kusumi, A. (2005). Fluorescence imaging for monitoring the colocalization of two single molecules in living cells. Biophys. J. *88*, 2126-2136.

Larkin, M.A., Blackshields, G., Brown, N.P., Chenna, R., McGettigan, P.A., McWilliam, H., Valentin, F., Wallace, I.M., Wilm, A., Lopez, R.*, et al.* (2007). Clustal W and Clustal X version 2.0. Bioinformatics *23*, 2947-2948.

Li, H., Robertson, A.D., and Jensen, J.H. (2005). Very fast empirical prediction and rationalization of protein pKa values. Proteins *61*, 704-721.

Liu, S.L., Sheng, R., O'Connor, M.J., Cui, Y., Yoon, Y., Kurilova, S., Lee, D., and Cho, W. (2014). Simultaneous in situ quantification of two cellular lipid pools using orthogonal fluorescent sensors. Angew. Chem. Int. Ed. Engl. *53*, 14387-14391.

Lorber, D.M., and Shoichet, B.K. (1998). Flexible ligand docking using conformational ensembles. Protein Sci. *7*, 938-950.

MacKerell, A.D., Bashford, D., Bellott, M., Dunbrack, R.L., Evanseck, J.D., Field, M.J., Fischer, S., Gao, J., Guo, H., Ha, S.*, et al.* (1998). All-atom empirical potential for molecular modeling and dynamics studies of proteins. J. Phys. Chem. B *102*, 3586-3616.

Nayal, M., and Honig, B. (2006). On the nature of cavities on protein surfaces: application to the identification of drug-binding sites. Proteins *63*, 892-906.

Pellecchia, M., Montgomery, D.L., Stevens, S.Y., Vander Kooi, C.W., Feng, H.P., Gierasch, L.M., and Zuiderweg, E.R. (2000). Structural insights into substrate binding by the molecular chaperone DnaK. Nat. Struct. Biol. *7*, 298-303.

Petrey, D., and Honig, B. (2003). GRASP2: visualization, surface properties, and electrostatics of macromolecular structures and sequences. Methods Enzymol. *374*, 492-509.

Pettersen, E.F., Goddard, T.D., Huang, C.C., Couch, G.S., Greenblatt, D.M., Meng, E.C., and Ferrin, T.E. (2004). UCSF Chimera--a visualization system for exploratory research and analysis. J. Comput. Chem. *25*, 1605-1612.

Rocchia, W., Alexov, E., and Honig, B. (2001). Extending the Applicability of the Nonlinear Poisson-Boltzmann Equation: Multiple Dielectric Constants and Multivalent Ions. J. Phys. Chem *B 105*, 6507-6514.

Rostkowski, M., Olsson, M.H., Sondergaard, C.R., and Jensen, J.H. (2011). Graphical analysis of pH-dependent properties of proteins predicted using PROPKA. BMC Struct. Biol. *11*, 6.

Sali, A., and Blundell, T.L. (1993). Comparative protein modelling by satisfaction of spatial restraints. J. Mol. Biol. *234*, 779-815.

Sheng, R., Chen, Y., Yung Gee, H., Stec, E., Melowic, H.R., Blatner, N.R., Tun, M.P., Kim, Y., Kallberg, M., Fujiwara, T.K.*, et al.* (2012). Cholesterol modulates cell signaling and protein networking by specifically interacting with PDZ domain-containing scaffold proteins. Nat Commun *3*, 1249.

Sippl, M.J. (1993). Recognition of errors in three-dimensional structures of proteins. Proteins *17*, 355-362.

Soto, C.S., Fasnacht, M., Zhu, J., Forrest, L., and Honig, B. (2008). Loop modeling: Sampling, filtering, and scoring. Proteins *70*, 834-843.

Stahelin, R.V., and Cho, W. (2001). Differential roles of ionic, aliphatic, and aromatic residues in membrane-protein interactions: a surface plasmon resonance study on phospholipases A2. Biochemistry *40*, 4672-4678.

Varnai, P., Thyagarajan, B., Rohacs, T., and Balla, T. (2006). Rapidly inducible changes in phosphatidylinositol 4,5-bisphosphate levels influence multiple regulatory functions of the lipid in intact living cells. J. Cell Biol. *175*, 377-382.

Wei, B.Q., Baase, W.A., Weaver, L.H., Matthews, B.W., and Shoichet, B.K. (2002). A model binding site for testing scoring functions in molecular docking. J. Mol. Biol. *322*, 339-355.

Wu, E.L., Cheng, X., Jo, S., Rui, H., Song, K.C., Davila-Contreras, E.M., Qi, Y., Lee, J., Monje-Galvan, V., Venable, R.M.*, et al.* (2014). CHARMM-GUI Membrane Builder toward realistic biological membrane simulations. J. Comput. Chem. *35*, 1997-2004.

Xiang, Z., Soto, C.S., and Honig, B. (2002). Evaluating conformational free energies: the colony energy and its application to the problem of loop prediction. Proc Natl Acad Sci U S A *99*, 7432-7437.

Yoon, Y., Lee, P.J., Kurilova, S., and Cho, W. (2011). In situ quantitative imaging of cellular lipids using molecular sensors. Nat Chem *3*, 868-874.